Earthquake Swarms on Transform Faults

Journal:	*Geophysical Journal International*
Manuscript ID:	draft
Manuscript Type:	Research Paper
Date Submitted by the Author:	n/a
Complete List of Authors:	Roland, Emily; Woods Hole Oceanographic Institution, Marine Geology and Geophysics; Massachusetts Institution of Technology, Earth Atmospheric and Plaetary Science McGuire, Jeff; Woods Hole Oceanographic Institution; Woods Hole Oceanographic Institution, Geology and Geophysics
Keywords:	Transform faults < TECTONOPHYSICS, Earthquake source observations < SEISMOLOGY, Creep

Earthquake Swarms on Transform Faults

Emily C. Roland[1]
Jeffrey J. McGuire[2]

[1] *MIT-WHOI Joint Program*
Woods Hole Oceanographic Inst.
MS # 24, Woods Hole, MA 02543, USA
E-mail: eroland@mit.edu
Phone: 1-508-289-3746

[2] *Woods Hole Oceanographic Institution*
Department of Geology and Geophysics
MS #24, Woods Hole, MA 02543, USA
E-mail: jmcguire@whoi.edu
Phone: 1-508-289-3290

submitted to *Geophys. J. Int.*

Earthquake Swarms on Transform Faults

Emily C. Roland[1] and Jeffrey J. McGuire[2]

[1] *MIT-WHOI Joint Program, Woods Hole, MA* 02543*, USA*

[2] *Woods Hole Oceanographic Institution, Woods Hole, MA* 02543*, USA*

SUMMARY

Swarm-like earthquake sequences are commonly observed in a diverse range of geologic settings including volcanic and geothermal regions as well as along transform plate boundaries. They typically lack a clear mainshock, cover unusually large regions relative to their total seismic moment release, and fail to decay in time according to standard aftershock scaling laws. Swarms often result from a clear driving phenomenon, such as a magma intrusion, but most lack the necessary geophysical data to constrain their driving process. To identify the mechanisms that cause swarms on strike-slip faults, we use relative earthquake locations to quantify the spatial and temporal characteristics of a set of swarms along Southern California and East Pacific Rise transform faults. Swarms in these regions exhibit distinctive characteristics, including a relatively narrow range of hypocentral migration velocities, on the order of a kilometer per hour. This rate corresponds to the rupture propagation velocity of shallow creep transients that are sometimes observed geodetically in conjunction with swarms, and is significantly faster than the earthquake migration rate associated with fluid diffusion. The uniformity of migration rates and low effective stress drops observed here suggest that shallow aseismic creep transients are the primary process driving swarms on strike-slip faults. Moreover, the migration rates are consistent with laboratory values of the rate-state friction parameter b (0.01) as long as the Salton Trough faults fail under hydrostatic conditions.

Key words: transform faults, earthquake source observations, creep

1 INTRODUCTION

The term *earthquake swarm* typically refers to a cluster of moderate earthquakes that occur over a period of hours to days without a distinct mainshock. In regions of magma intrusion and CO_2 degassing, swarms have been linked to fluid-flow processes that alter the stress field and trigger seismicity (Hill 1977; Smith, et al. 2004; Hainzl & Ogata 2005). However, with recent improvements in seismic observation capabilities, it is becoming clear that swarms occur in a variety of tectonic settings, not just in areas of volcanism. High rates of seismic swarms have been observed historically in the southern region of the San Andreas transform fault system, where it extends into the Salton Trough in Southern California (Richter 1958; Brune & Allen 1967; Johnson & Hadley 1976). Recent studies of high-quality earthquake catalogs have demonstrated that swarms are a common feature of various large-scale tectonic fault systems including those in California and Japan (Vidale & Shearer 2006; Vidale, et al. 2006). Additionally, analysis of aftershock productivity and foreshock occurrence rates on mid-ocean ridge transform faults indicate that oceanic sequences are generally more swarm-like than typical sequences on continental strike-slip boundaries (McGuire, et al. 2005).

Although in may cases, geophysical observations are not available to constrain the specific process, certain swarm seismicity characteristics reflect an underlying driving mechanism that is fundamentally different from mainshock-aftershock Coulomb stress triggering. Earthquake swarms are often characterized by an effective seismic stress drop (the ratio of total seismic moment release to fault area) that is an order of magnitude lower than stress drop values typical for mainshock-aftershock sequences on strike-slip faults (Vidale & Shearer 2006). Empirical laws developed from observations of aftershock sequences triggered from a single large event also do a poor job of fitting swarms on transform boundaries. Omori's Law of seismicity rate decay following a mainshock (Omori 1894) and Båth's law, which describes the difference in the magnitude of a mainshock and its largest aftershock (Helmstetter & Sornette 2003b), cannot be applied to earthquake swarm seismicity with values typical of continental strike-slip fault systems. Observations of unusual temporal and spatial seismicity patters associated with swarms can also be extended to earthquake sequences on the East Pacific Rise (EPR). In their study of oceanic transform seismicity, McGuire et al. (2005) showed that foreshocks are an order of magnitude more common on EPR transform faults than on faults in California, while aftershocks are an order of magnitude less common. This analysis demonstrated that EPR transform seismicity cannot be explained by typical earthquake triggering models, and went on to suggest that an aseismic driving process was likely responsible for the increased foreshock activity. Forsyth et al. (2003), inferred an anomalously low stress drop associated with a swarm on the western boundary of the Easter Microplate. Based on unusual spatial properties, aseismic slip events were similarly hypothesized to trigger the swarm seismicity in that analysis.

A few studies have directly associated swarms on transform faults with geodetically observed aseismic creep. On the central San Andreas, Linde et al. (1996) used creepmeter observations to connect a small number of earthquakes with magnitude ∼5 creep events that had time scales of a few days. Lohman and McGuire (2007) studied a large swarm in the Salton Trough using both seismic and geodetic data, and inferred that the magnitude of surface deformation that occurred during the swarm could not be explained by the recorded seismicity alone. Their modeling of the observed deformation required a significant contribution from shallow aseismic creep coincident with the swarm. A hypocentral migration velocity on the order of 0.1-1.0 km/hr, which was observed during the early stage of the Lohman and McGuire sequence, is a common feature of strike-slip swarms in the Salton Trough (Johnson & Hadley 1976). This velocity is consistent with estimated rupture propagation speeds of creep events in California (King et al. 1973; Burford 1977; Linde 1996; Glowacka et al. 2001), and is significantly faster than the migration rate of earthquakes observed in regions of CO_2 degassing and borehole fluid injections. Seismicity initiated by fluid overpressure tends to reflect fluid diffusion time scales, with earthquakes spreading spatially proportional to $t^{1/2}$ and migration velocities not exceeding fractions of a kilometer per day (Audigane et al. 2002; Hainzl & Ogata 2005; Shapiro et al. 2005). Based on the the wide disparity between migration rates associated with fluid diffusion and aseismic slip, hypocentral migration velocities observed during seismic swarms may be used to infer the specific stress transfer mechanism driving seismicity, even if direct observational evidence of the mechanism is not available.

Here, we continue to investigate the physical mechanisms that cause earthquake swarms, and explore the possibility that swarms are generally associated with aseismic creep on strike-slip plate boundaries. In this study, seven swarms are analyzed from Southern California and EPR transform faults. Reliable earthquake locations are derived and used to identify spatial migration patterns, which are taken as a proxy for the physical triggering mechanism driving the sequences. We employ temporal characteristics of the moment release to develop an objective definition of an earthquake swarm, and identify spatial moment release characteristics that are common to most swarms in our data set. We utilize the effective stress drops and hypocentral migration rates to constrain the potential mechanism causing swarms on strike-slip faults in Southern California and the East Pacific Rise, and compare our results to predictions calculated from rate-state friction and crack propagation models.

2 DATA & METHODS

We systematically explore the physical mechanisms causing tectonic swarms by analyzing a number of sequences from the Salton Trough and EPR. Owing to the vast difference in the quality and density of seismic data available, sequences from these two regions are analyzed with different relocation

methods. Seven earthquake sequences are analyzed in total: three in Southern California that have accurate relocations available from prior studies, one in Southern California that we relocate using body waves recorded by local arrays and three EPR sequences that are detected and located using teleseismic surface wave arrivals at Global Seismic Network (GSN) stations. Using locations and magnitudes, we estimate the effective stress drop and along-fault hypocentral migration rate of each swarm. We also calculate the skew of the temporal history of seismic moment release for each episode, which is a quantitative way of distinguishing swarms from aftershock sequences. Below we describe the details of each type of calculation.

2.1 Southern California seismicity: body-wave relocations

For each Southern California swarm analyzed here, relative hypocentral locations were derived using body wave arrival times from local seismometer arrays. A swarm in 1975 was relocated by Johnson & Hadley (1976), and locations were derived for two swarms in 1981 and 2005 by Lohman & McGuire (2007). We utilize estimates of migration velocity from these two analyses. For the 1981 and 2005 swarms, burst-radii were calculated here, using the Lohman & McGuire locations, as the mean of the distance of each event to the spatial centroid of the sequence. The burst radius of the 1975 swarm was calculated in the same manner from the Southern California Earthquake Data Center (SCEDC) catalog locations. For a swarm on the Imperial Fault in 2003, arrival time data was combined from two catalogs to determine relative relocations using the double-difference algorithm (Waldhauser & Ellsworth 2000). Arrival time picks from the Southern California Seismic Network (SCSN) were combined with arrivals from the RESNOM network, maintained by the *Centro de Investigación Científica y de Educación Superior de Ensenada* (CICESE), which provided additional azimuthal coverage south of the US-Mexico border. For the double-difference relocations, we required event arrival pairs to be observed at a minimum of 8 stations within 500 km and separated by no more than 5 km. We employed a one-dimensional velocity model appropriate for the Salton Trough, which was extracted from the Southern California Earthquake Center's 3D unified Southern California reference velocity model, version 4 (Magistrale et al. 2000).

2.2 EPR seismicity: surface-wave relocation

We analyze three swarms from transform faults on the EPR and the Galapagos Ridge using a surface-wave earthquake detection and location method that makes use of Rayleigh wave empirical Green's functions (EGFs). In the frequency band between 0.02 and 0.05 Hz, first-orbit Raleigh (R1) waves have a high signal-to-noise ratio and a group velocity that is fairly constant for young oceanic lithosphere, around 3.7 km/s (Nishimura & Forsyth 1988). This allows arrival times to be interpreted in terms of

source location differences rather than dispersion (Forsyth et al. 2003). Waveforms from individual earthquakes on the same fault are essentially identical, and at low frequencies the amplitude of the waveforms scale with the moment of the earthquake. We identify and locate swarm events relative to an EGF based on their correlation coefficients and differential arrival times from a set of azimuthally distributed GSN stations. The magnitude and location of the selected EGF are taken from the Global Centroid Moment Tensor (CMT) catalog directly when a CMT solution is available for one of the earthquakes in the sequence. If a moment calculation is not available, one of the large earthquakes in the sequence is cross-corelated with an appropriate CMT catalog event from the same fault to determine its seismic moment. That event is used as the EGF for the rest of the event locations. All of the EGF events used here are greater than $M_w 4.7$.

Two swarms that occurred on the Galapagos Ridge transform in 2000 and the Siqueiros transform in 2001 were detected by an array of autonomous hydrophones operated by NOAA, moored in the eastern equatorial Pacific (Fox et al. 2001). The earthquake catalogs derived from t-phases recorded by these hydrophones have a detection threshold of approximately $M_w 3$, and we utilized these catalogs for identifying the source times of large events within the swarm. Magnitude estimates from the hydroacoustic catalogs are unreliable however, owing to complicated wave phenomena and the high-frequency energy of the t-phase (McGuire 2008). To determine reliable M_w estimates and locations, GSN waveforms for each t-phase event were extracted from a number of stations, bandpass filtered and cross correlated with the EGF R1 waveform. Relative event locations were then obtained by fitting a cosine function to the differential R1 arrival times using an L1-norm fit. Best-fit cosine scale and phase parameters characterize the distance and azimuth of the earthquake relative to the Green's function event (McGuire 2008). The location error is estimated using a bootstrap algorithm that assumes a Gaussian distribution with a 1 second standard deviation for the differential travel-time measurement errors (Shearer 1997; McGuire 2008). For the 2007 Gofar transform swarm, no events were detected by standard teleseismic catalogs. One of the sequence events was utilized as the EGF after its moment was first estimated relative to a nearby CMT event; the CMT event was used as a preliminary Green's function for the single EGF moment calculation. The other events in the swarm were then detected by cross correlating the EGF waveform with seismograms from several GSN stations. Individual events were identified in the cross-correlation process as arrivals with a high cross-correlation coefficient at a sufficient number of stations to ensure azimuthal coverage. The relative locations of these newly detected events were determined using the same procedure as for the Galapagos and Siqueiros swarms.

2.3 Skew of moment release

Seismic swarms are distinguished from typical mainshock-aftershock sequences by their unique seismicity patterns: the largest swarm events tend to occur later in the sequence, swarms contain several large events as opposed to one clear mainshock, and elevated swarm seismicity is more prolonged in time (Fig. 2). Swarms thus deviate from established triggering models developed for aftershock sequences, such as Omori's law, which describes the decay rate of earthquakes following a mainshock (Omori 1894). Because of these deviations, quantitative earthquake triggering models such as the Epidemic Type Aftershock Sequence (ETAS) model (Ogata 1988) do not provide a good fit to the temporal evolution of moment release during a swarm (Llenos & McGuire 2008). One simple way to quantitatively identify earthquake clusters with swarm-like properties is through characterizing the timing of the largest earthquakes relative to the rest of the seismicity. To accomplish this, we calculate the skew of the seismic moment release history (i.e. the normalized third central moment) for each of the sequences that we analyze.

To calculate a skew value for a given sequence from its moment release history, we define the duration of the swarm as the period of time during which the seismicity rate is at least 20% of its maximum value. The rate is calculated here using two-hour time bins. The moment release history, $F(t)$, is normalized so that within the determined time period of heightened seismicity $\lim_{t\to\infty} F(t) = 1$. The third central moment is then calculated as an integral over the duration of the sequence:

$$\bar{\mu}_3 = \int (t - t^*)^3 dF(t), \tag{1}$$

where t^* is the centroid time (Jordan 1991). The normalized third central moment represents the skew of seismic moment release, and is equal to the third central moment divided by the square root of the variance. Skew values quantitatively reflect the temporal evolution of the moment release during an earthquake sequence, with a value of zero for a symmetric sequence, a negative value for a sequence that begins slowly and ends abruptly, or a positive value for a sequence that begins abruptly and decays slowly, such as a typical mainshock-aftershock sequence. This value serves as a rough way of quantitatively differentiating swarm-like sequences from mainshock-aftershock sequences (*see discussion section*).

2.4 Stress Drop

To differentiate swarm and aftershock sequences based on their spatial properties, we calculate an effective seismic stress drop for each sequence. While stress drop values for large strike-slip earthquakes are on the order of 10 MPa (Abercrombie & Rice 2005), the effective stress drop of swarms in Southern California tends to be an order of magnitude lower than mainshock-aftershock sequences

(Vidale & Shearer 2006). We estimate the effective stress drop for each swarm using the approach of Vidale & Shearer (2006), where a rupture area is estimated for an earthquake sequence from a burst radius, which is calculated as the mean distance from each event to the spatial centroid of the cluster. We assume a vertical strike-slip fault for the oceanic sequences and a circular fault for the smaller Southern California sequences with reliable depth estimates. An area estimate is made using the burst radius and is used along with the cumulative moment to calculate a stress drop, $\Delta\sigma$, again assuming either a circular fault:

$$\Delta\sigma = \frac{7\pi}{16}\mu\frac{\bar{D}}{a}, \tag{2}$$

or a rectangular fault:

$$\Delta\sigma = \frac{2}{\pi}\mu\frac{\bar{D}}{w}, \qquad \text{with } \bar{D} = \frac{M_o}{\mu S} \tag{3}$$

(Kanamori & Anderson 1975). Here, μ is the shear modulus, $\bar{D}$ is the average slip, a is the burst radius, w is the seismic width, which we assume to be 5 km on the EPR transforms (Trèhu & Solomon 1983) and $S = 2aw$ is the fault area.

3 RESULTS

3.1 1975 Brawley Swarm

In 1975 a large earthquake swarm occurred in the NW-striking Brawley seismic zone, just south of the Salton Sea. This swarm was analyzed by Johnson and Hadley (1976) using data recorded by 16 short-period instruments that were part of the USGS Imperial Valley array. Two hundred and sixty four events spanning 8 days were located; the relative occurrence times and magnitudes of these events are displayed in the first panel of Fig. 2. Brawley swarm event locations exhibit bilateral migration, spreading outward at a rate of approximately 0.5 km/hr (Johnson & Hadley 1976). A source model involving the propagation of a right-lateral creep event was hypothesized as an explanation for the hypocentral migration. Johnson and Hadley cited a number of observations as support for this model, including an increase in detected shallow seismicity directly before the onset of the swarm, as well as the existence of seismically quiescent fault segments in the region.

During the 1975 Brawley swarm, elevated seismicity levels persisted for over 100 hours after the largest events. Moment release that, in this way, is uniquely prolonged in time is reflected in a large skew value of +20 (Table 1). Including the largest event, there were 6 earthquakes with moment magnitudes between 4.0 and 4.7. The effective stress drop calculated for this sequences based on 162 SCEDC catalog locations was 0.2 MPa, with a burst radius of 4.5 km. Our estimate of burst radius

is roughly consistent with the Johnson and Hadley estimate of the swarm's spatial extent, which was determined using local network data.

3.2 West Moreland and Obsidian Buttes Swarms

The 1981 West Moreland swarm and 2005 Obsidian Buttes swarm both occurred within the Brawley Seismic Zone. Events associated with these sequences were recorded by the Southern California Seismic Network and were the focus of the study by Lohman & McGuire (2007). Peak seismicity during the West Moreland swarm spanned more than 3 days, and seismicity was elevated above the background rate for over 130 hours before the occurrence of the largest event, a M_w 5.9. Swarm events demonstrate bilateral hypocentral migration at a rate of about 1.0 km/hr, spreading outward along a 15 km section of the NE-trending fault segment (Fig. 3). A few hours after the largest earthquake, events began migrating onto a north-south trending fault, 10 km to the north, at a rate of about 0.5 km/hr. Similar to the West Moreland swarm, bilateral migration was observed during the multiple day Obsidian Buttes swarm. During the first 15 hours, earthquake hypocenters spread bilaterally at a rate of approximately 0.5 km/hr along the northeast-striking fault (Fig. 4). Deformation associated with this swarm was also observed geodetically, using InSAR observations, as well as recordings from two nearby Southern California Integrated GPS Network (SGIGN) stations. An inversion of the InSAR data demonstrated that significant shallow aseismic slip was required during the swarm to explain the extent of surface deformation (Lohman & McGuire 2007).

We calculate skew values of approximately -17 and -8 for the West Moreland and Obsidian Buttes swarms, respectively. These negative values result from a large amount of seismic release before the sequences' temporal centroid, which is essentially coincident with the largest event, and signify the ramping up of seismic activity before the largest events occur. The effective stress drop for each these sequences was estimated at 1.28 and 3.75 MPa, again values that are relatively low compared to effective stress drop values typical of large mainshocks in the region.

3.3 2003 Imperial Fault Swarm

In May 2003, an earthquake swarm occurred on a NE-striking fault within the Imperial Fault Zone. During this sequence, seismic activity was elevated for approximately 30 hours, with the largest earthquake, a M_w 3.8, occurring about 9 hours after the onset of elevated seismicity. Arrival times from the Mexican RESNOM and Southern Californian SCSN catalogs were combined and used to relocate swarm events. About ten thousand P- and S-wave arrivals observed from a combination of 46 Californian and Mexican stations were used to relatively relocate 51 earthquakes (Fig. 5b). Event hypocenters focus onto a fault plane approximately 3 km long, with location errors of 10 meters based

on the SVD error analysis. Events of this sequence also demonstrate northward hypocentral migration along the fault, at a rate between 0.1 and 0.5 km/hr (Fig. 5c). The skew value calculated for the Imperial Fault swarm moment release is -2, again reflecting a pattern of abundant small-magnitude seismicity ramping up to the largest events. The effective stress drop was estimated at 0.18 MPa.

3.4 2000 Galapagos Swarm

In October of 2000 a seismic swarm was recorded on a left-lateral transform fault offsetting the Galapagos Ridge, just north of the Galapagos Islands. One hundred and thirty eight t-phase arrival times associated with the two-day swarm were recorded by the NOAA hydrophone array deployed in the eastern Pacific Ocean (Fox et al. 2001). Approximately 5 hours after the onset of the swarm, a M_w 5.2 event occurred, followed by a decrease in moment release rate until approximately hour 12, when a doublet (M_w 5.7 and 5.5) occurred. These were followed a few hours later by the largest event, a M_w 5.9. In total, 30 events greater than M_w 4.0 occurred before the seismicity rate abruptly returned to background levels approximately 36 hours after the swarm began.

Events associated with this swarm were located relative to an EGF which occurred on 10/21 at 15:52:53 UTC using the surface wave relative relocation method (*see Methods section*) with GSN waveform data from 19 stations. The EGF was the largest event of the sequence with a Global CMT magnitude of M_w 5.9. Twelve events with the best centroid inversions have been used here to analyze the spatial characteristics of this swarm (Fig. 6). Based on locations derived using this method, bilateral migration along the transform has been inferred at a rate between 0.1 and 1.0 km/hr. (Fig. 7)

Seismicity associated with the Galapagos swarm was also recorded by an 11 station broadband seismometer array, deployed on the Galapagos Islands (Hooft et al. 2003). Although the land-based seismometer array, located entirely to the south of the fault, and the hydrophone array, located entirely to the west of the fault, were not well placed for recovering Galapagos Ridge earthquake locations, they were useful for determining event magnitudes with a higher degree of accuracy than can be achieved from teleseismic data. Love-wave arrivals from rotated radial-component records were identified using an EGF technique similar to that used with the teleseismic R1-arrivals, as described above. One hundred and nine events were detected with cross-correlation coefficients greater than 0.7 from seismograms filtered to 0.03-0.08 Hz. Magnitude estimates for these events are displayed in Fig. 7a as black symbols. Based on this data set we calculated a skew of -4 reflecting the significant amount of moment release before the largest event of the sequence. The cumulative moment from the Love-wave magnitude estimates was used with the burst-radius from surface-wave relocations to determine an effective stress drop of 1.0 MPa.

3.5 2001 Siqueiros Swarm

A large earthquake sequence on the Siqueiros transform fault in April of 2001 was detected by the eastern Pacific NOAA hydroacoustic array (Fox et al. 2001). One hundred and seventy t-phase events associated with the 2001 sequence were observed by hydrophones; these events had locations corresponding to the S2 and S3 segments of the Siqueiros fault (Gregg et al. 2006). The largest event was a M_w5.7, as calculated in the Global CMT catalog, which occurred very early in the sequence. With the CMT event as the Green's function, 13 events with magnitudes greater than 4.2 were detected and located using the surface-wave location method. Seismograms used in the centroid location inversions came from 21 GSN stations that were bandpass filtered to 0.02-0.04 Hz. Earthquake centroids clearly locate onto the two fault segments, however the spatial evolution of seismicity during the sequence is difficult to interpret (Fig. 8). During the first 8 hours following the largest event, centroids migrated from west to east along the S3 segment of the Siqueiros fault, corresponding to the first 45 t-phase events. Seismicity then became active on the S2 segment to the west, and again migrated east for the remainder of the episode. These two fault segments are separated by an inter-transform spreading center (ITSC). Gregg et al. (2006) proposed that some of the later seismicity to the west actually occurred on secondary normal faults flanking the ITSC. While this may account for some of the smaller seismicity seen in the t-phase data, based on the surface wave locations and waveform similarity, the large events occurred as right-lateral strike-slip earthquakes, similar to the CMT catalog event. The skew of the Siqueiros sequence is positive, around 5, reflecting the occurrence of the largest event early in the sequences, followed by prolonged seismic activity. The total stress drop from earthquakes on both segments was calculated at approximately 1.0 MPa.

3.6 2007 Gofar Swarm

The Gofar transform fault is the southernmost, and most seismically active of the Quebrada-Discovery-Gofar fault system that offsets the EPR at approximately 4°South. On 12/28 2007, an earthquake sequence was recorded on the western segment of the Gofar transform, lasting approximately 2 days. Events associated with this sequence were detected and located using the R1 surface-wave method, with data from 15 GSN stations. The location and magnitude of the empirical Green's function event used in this analysis were calculated relative to a CMT event that occurred on the same fault segment in 2003. The EGF used for locating the remainder of the sequence events was a M_w5.3 that occurred on 12/29 at 00:48:00, approximately 5 hours after the initiation of the sequence. The 13 events with the best locations focus onto a 30 km long segment of the fault (Fig. 9). It is apparent from the surface-wave derived locations that event centroids migrated to the east at a rate of 0.5-1.0 km/hr. This sequence has a skew of +5 and a stress drop of approximately 0.2 MPa.

3.7 Southern California Distributed Seismicity

In order to develop a basis for comparison in our analysis of earthquake swarms on transform boundaries, we combine our findings from the seven moderate-sized recent and historical sequences described above, to those recently published by Vidale and Shearer (2006). In their analysis of small seismicity clusters (burst radius < 2 km) in Southern California, 71 seismic bursts were identified using data from the SHLK_1.01 catalog of cross-correlation relocations (Shearer et al. 2005). Fourteen of these events were classified as aftershock sequences on the basis that they began with their largest event, and 18 events were identified as swarm-like, based on various qualitative factors. Specifically, swarms were recognized as episodes with the largest events occurring later into the sequence, large spatial extents relative to the largest earthquake (implying a low stress drop), and in many cases, a systematic spatial evolution of hypocenters, spreading either outward along the fault or linearly in one direction with time. We calculate skew and stress drop values for the 14 aftershock and 18 swarm-like sequences in the Vidale and Shearer data-set; these are displayed in Fig. 10 along with values calculated for the other seven swarms presented above. Swarm-like sequences characterized using these parameters, cluster toward the low stress drop-low skew quadrant of the plot, with an occasional anomalously high skew outlier, like that associated with the Brawley swarm. Aftershock sequences, meanwhile, cluster fairly regularly into the quadrant representative of higher stress drops and small positive skew values, usually around zero and not more than 5, which reflect established empirical triggering patterns such as Omori's Law. These quantitative parameters correspond well with the Vidale and Shearer observational classification of a sequence being "swarm-like", based on the long duration and lack of an initiating mainshock, as well as the large spatial extent.

4 DISCUSSION

Our analyses of the spacial and temporal characteristics of swarms on Southern California and East Pacific Rise transform faults expose three distinct properties of these sequences that signify a consistent physical driving mechanism. Low effective stress drops, deviation of the temporal evolution of moment-release from typical scaling laws, and migration velocities of 0.1-1.0 km/hr are all consistent with a model in which aseismic fault slip modifies the stress-field and triggers swarm seismicity. Historical surface deformation observations as well as recent geodetic studies in the Salton Trough have noted a prevalence of shallow creep events (Lyons et al. 2002; Lyons & Sandwell 2003; Lohman & McGuire 2007), demonstrating the feasibility of this mechanism for the Southern California faults. There have been no direct geodetic observations of creep on EPR transform faults, but it is well doc-

umented that oceanic transforms must have a significant component of aseismic fault slip (Bird et al. 2002; Boettcher & Jordan 2004), making creep a plausible explanation for the EPR swarms as well.

Many of the sequences examined here display a gradual ramping-up of moment release, with the largest events occurring late in the sequence, and seismicity that is prolonged in time relative to Omori-like decay. These characteristic features of seismic swarms are manifest into negative or sometimes anomalously high positive skew values relative to those associated with aftershock sequences (Fig. 10). The Epidemic-Type Aftershock Sequence (ETAS) model (Kagan & Knopoff 1991) combines a number of empirical triggering laws, including Omori's Law, and has been used to represent the normal occurrence rate of earthquakes triggered by previous events (Ogata 1988; Helmstetter & Sornette 2003a). We infer that anomalously low or high skew values indicate earthquake sequences that conform to different moment release patterns and cannot be fit by the ETAS model (Ogata 2005). Anomalous skew values should indicate periods of time when seismicity deviates from aftershock-like Coulomb stress-triggering patterns, and is driven instead by a transient stressing event. In Fig. 11, ETAS-predicted seismicity is optimized over the 26-month time period preceding the large swarm in 2000 on the Galapagos Ridge transform fault. Predicted seismicity is displayed as a straight line in ETAS-transformed time (red line). Transformed time represents the amount of time predicted to elapse before the next seismic event, based on the background seismicity rate and the seismic history. ETAS trigging parameters, derived here as the maximum likelihood fit based on events greater than 3.6 (the magnitude threshold of our surface-wave derived catalog), are fairly typical values of background seismicity rate, $\mu = 0.03$ and local seismicity parameters $c = 0.01$ and $k = 0.3$, with the Omori time decay parameter, p, constrain to 1.0 (Bohnenstiehl et al. 2002) and moment-distribution exponent, α, constrained to 0.8 (Boettcher & Jordan 2004). The observed seismicity (blue line) deviates significantly from that which is predicted using these parameters during the period of the swarm (shaded region). Early in the sequence, the cumulative number of observed earthquakes far exceeds the ETAS-prediction, and then following the largest swarm event, shows a relatively diminished rate (slope of the blue line). It is interesting to note that the final cumulative number of events that actually occurs on this fault over the multiple year time span is significantly less than that predicted for a fault exhibiting ETAS-like aftershock sequences, despite the accelerated rate observed early in the 2000 swarm. Anomalous skew values, like the -5 skew of the Galapagos swarm, reflect these types of deviations, and indicate a triggering phenomenon that cannot be represented by empirical laws that emulate aftershock seismicity.

Low effective stress drop values characteristic of swarms also provide evidence for a unique driving process. Values calculated for sequences here, on the order of 0.1-1.0 MPa, are significantly lower than values for typical mainshock-aftershock sequences of similar size (i.e. 2-10 MPa). Recently,

Brodsky and Mori (2007) demonstrated that creep events have lower stress drops than ordinary earthquakes, on the order of 0.1 MPa. Low effective stress drop values for swarms determined in this study are thus consistent with values that would be expected for aseismic creep events. Assuming the 0.1 MPa value applies to creep events driving the EPR swarms as well, we can roughly estimate the magnitude of the aseismic slip. For the example of the Gofar sequence, with a fault length, $L = 30$ km, width $w = 5$ km and stress drop $\Delta\sigma = 0.1$ MPa we find an aseismic moment release of approximately M_w5.3. While this is clearly only a first order estimate, it suggests that aseismic slip during the EPR swarms would be comparable in size to the seismic component, roughly agreeing with the long-term partitioning of slip between the two failure modes as seen in global studies of the slip deficit on oceanic transforms (Bird et al. 2002; Boettcher & Jordan 2004).

The relatively narrow range of spatial migration velocities between 0.1 and 1.0 km/hr may be the most direct evidence of aseismic fault slip. Observations of seismicity triggered by borehole fluid injection (Audigane et al. 2002; Shapiro et al. 2005) and subsurface fluid flow from magma degassing (Hainzl & Ogata 2005) consistently show earthquake hypocenters that spread following much slower pore-pressure diffusion, with distances that increase proportional to $t^{1/2}$ at rates not exceeding meters per day. Based on the migration rates seen here, the Salton Trough and EPR swarms are most likely not caused by fluid-flow transients. Geodetic observations further rule out magma intrusion in favor of fault slip (Lohman & McGuire 2007). Limited geodetic observations of propagation speeds associated with slow earthquakes and aseismic creep events are, to first order, consistent with migration rates between 0.1-1.0 km/hr. Studies using creepmeters to observe creep events on the San Andreas, Calaveras and Hayward faults determine propagation speeds on the order of 10 km/day (0.4 km/hr) (King et al. 1973; Burford 1977). More recently, borehole strainmeter observations of a slow earthquake sequence on the San Andreas were found to be consistent with rupture propagation rates between 0.2-0.35 m/s (0.7-1.3 km/hr) (Linde 1996). In the Salton Trough, creep events from the Cerro Prieto step-over at the southern end of the Imperial fault have been observed with a rupture propagation velocity of 4 cm/s (0.14 km/hr) using multiple creep meters (Glowacka et al. 2001). While data on creep event rupture propagation velocity is limited due to sparse instrumentation, values from strike-slip faults in California and Mexico are within the range of our observations of seismicity migration rates.

Theoretical expressions relating stress drop, rupture propagation velocity and slip velocity provide the final link between earthquake swarms and aseismic creep events. Ida (1973) and Ohnaka and Yamashita (1989) derived a relation between maximum slip velocity, v_{max}, and rupture propagation velocity, v_r, for a mode II shear rupture propagating with a constant velocity of the form:

$$v_{max} = \gamma \frac{\Delta\sigma_b}{\mu} v_r. \tag{4}$$

Here, γ is a constant on the order of one and $\Delta\sigma_b$ is the breakdown stress drop, characterizing the

difference between the peak stress and stress at frictional sliding (Shibazaki & Shimamoto 2007). Rate-state friction models were used by Rubin and Ampuero (2007) to determine essentially the same relation for a propagating rupture front with a quasi-steady shape:

$$\frac{v_r}{v_{max}} = \frac{\mu}{\Delta\sigma}, \qquad and \quad \Delta\sigma = \frac{b\sigma}{\ln[v_{max}\theta/D_c]}, \tag{5}$$

with θ representing the 'state' ahead of the propagating front, D_c, the characteristic slip distance for state evolution, b, a lab-derived friction parameter that characterizes the drop in friction from peak to steady-state sliding levels and σ the effective normal stress. Using this relation for slip and rupture propagation velocity with approximate values derived from our analyses of swarm seismicity, $\Delta\sigma \sim 0.1$ MPa, $v_r \sim 0.5$ km/hr ~ 0.14 m/s (Table 1) and the shear modulus $\mu = 30$ GPa, we derive a maximum slip velocity, $v_{max} \sim 5 \times 10^{-7}$ m/s. This value is significantly slower than slip speeds during typical earthquakes, which are on the order of meters per second, but is comparable to surface displacement rates observed during creep events. On the Imperial fault, Glowacka et al. (2001) observed peak slip-rates using creep meters on the order of 100 mm/day (10^{-6} m/s) during creep transients. Based on these relations, as long as the dominant slip mode is aseismic creep ($v_{max} \sim 10^{-7}$ m/s) rather than seismic fault slip ($v_{max} \sim 1$ m/s), our estimates of stress drop and rupture propagation velocity provide a self-consistent model of fault failure with either crack or rate-state equations. These calculations are also consistent with observations of shallow aseismic creep in the Salton Trough. Combining our estimate of rupture propagation velocity ($v_r = 0.28$ m/s, for the Obsidian Buttes swarm), the observed slip velocity of Salton Trough creep events, $v_{max} \sim 10^{-6}$ m/s (Glowacka et al. 2001), laboratory values of $b \sim 10^{-2}$, a density of 2500 kg/m^3, an S-wave velocity of 2.7 km/s (i.e. a shear modulus of 19 GPa), and a representative value of $\ln[v_{max}\theta/D_c]$ of 5 (Rubin & Ampuero 2007) yields a normal stress of 33 MPa. This value matches the expected normal effective stress for hydrostatic conditions at a depth of 2.3 km. Lohman and McGuire (2007) found the peak aseismic slip during the Obsidian Buttes swarm occurred between depths of 1 and 3 km. We thus find that the observed rupture propagation velocity of the Salton Trough and EPR swarms and a slip velocity on the order of that assumed for aseismic creep are consistent with laboratory derived values of the rate-state friction parameter $b \sim 0.01$ (Kilgore et al. 1993) as long as the Salton Trough faults fail under hydrostatic conditions.

5 CONCLUSIONS

Based on our analysis of seismic swarms on Southern California and EPR transform faults, we have identified several parameters that point to aseismic creep as the likely driving mechanism for the recurrent swarms on these strike-slip plate boundaries. Swarms show a large spatial extent relative to

their cumulative seismic moment and a correspondingly low effective stress drop, a temporal evolution that is inconsistent with standard scaling laws and spatial migration speeds on the order of 0.1-1.0 km/hr. These characteristics are consistent with field observations of creep events as well as with theoretical models of fault slip at creep rates. Given the relative frequency of swarms in the Salton Trough and EPR, it appears likely that a significant fraction of moderate and large earthquakes on these boundaries are triggered by aseismic fault slip. Moreover, all three properties of swarms could be easily identified in real time if high precision locations were available. In view of the significant damage Salton Trough swarms have caused in the past, these systematic properties could be used to improve real-time hazard estimates by detecting the existence of a swarm-like sequence relatively early in its evolution and identifying the increased level of hazard compared to a typical aftershock sequence.

REFERENCES

Abercrombie, R. E., & Rice, J. R., 2005, Can observations of earthquake scaling constrain slip weakening, *Geophys. J. Int*. **162**, 406-424.

Ampuero, J. Rubin, A. M., 2008. *Earthquake nucleation on rate and state faults Aging and slip laws*. *J. Geophys. Res*. **113**, doi:10.1029/2007JB005082.

Audigane, P., Royer, J. J. & Kaieda, H., 2002,Permeability characterization of the Soultz and Ogachi large-scale reservoir using induced microseismicity, *Geophysics*. **67**, 204-211.

Bird, P., Kagan, Y.Y., & Jackson, D.D., 2002, Plate tectonics and earthquake potential of spreading ridges and oceanic transform faults, *Plate Boundary Zones, AGU Monograph*. Geodyn. Ser. vol. 30, edited by S. Stein and J. T. Freymueller, 203-218.

Boettcher, M. S. & Jordan, T. H., 2004, Earthquake scaling relations for mid-ocean ridge transform faults, *J. Geophys. Res.*. **109**(B12), doi:10.1029/2004JB003110.

Bohnenstiehl, D. R., Tolstoy, M., Dziak, R. P., Fox C. G., Smith, D. K., 2002, Aftershock sequences in the mid-ocean ridge environment: an analysis using hydroacoustic data, *Tectonophysics*. **354**, 49-70.

Brodsky, E. E., & Mori, J., 2007, Creep events slip less than ordinary earthquakes, *Geophys. Res. Lett*. **34**, doi: 10.1029/2007GL030917.

Brune, J. N. & Allen C. R., 1967, A low-stress-drop, low-magnitude earthquake with surface faulting: The Imperial, California, earthquake of March 4, 1966, *Bull. Seism. Soc. Am*. **57**, 501-514.

Burford, R. O., 1977, Bimodal distribution of creep event amplitudes on the San Andreas fault, California, *Nature*. **268**, 424-426.

Forsyth, D. W., Yang, Y., Mangriotis, M. D., & Shen, Y., 2003, Coupled seismic slip on adjacent oceanic transform faults, *Geophys. Res. Lett*. **30**(12), 1618, doi:10.1029/2002GL016454.

Fox, C. G., Matsumoto, H. & Lau, T. K. A., 2001, Monitoring Pacific Ocean seismicity from an autonomous hydrophone array, *J. Geophys. Res.*. **106**, 4183-4206.

Glowacka, E., Gonzalez, J. J., Nava, F. A., Farfan, F. & Díaz de Cossio, G., 2001, Monitoring surface deformation in the Mexicali Valley, BC, Mexico, *Paper presented at the 10th FIG International Symposium on Deformation Measurements*. Calif. Inst. of Technol., Orange, CA.

Gregg, P. M., Lin, J. & Smith, D. K., 2006, Segmentation of transform systems on the East Pacific Rise: Implications for earthquake processes at fast-slipping oceanic transform faults, *Geology*. **34**(B05S07), 289-292.

Hainzl, S. & Ogata, Y., 2005, Detecting fluid signals in seismicity data through statistical earthquake modeling, *J. Geophys. Res.*. **110**(B05S07), doi:10.1029/2004JB003247.

Helmstetter, A., Sornette, D., 2003, Importance of direct and indirect triggered seismicity in the ETAS model of seismicity, *Geophys. Res. Lett.*. **30**, 11, 1576-1579.

Helmstetter, A., Sornette, D., 2003, Bath's law Derived from the Gutenberg-Richter law and from Aftershock Properties , *J. Geophys. Res.*. **30**(20), 2069, doi:10.1029/2003GL018186.

Helmstetter, A., Sornette, D., 2002, Subcritical and supercritical regimes in epidemic models of earthquake aftershocks, *J. Geophys. Res.*. **107**(B10), 2237, doi:10.1029/2001JB001580.

Hill, D. P., 1977, A model for earthquake swarms, *J. Geophys. Res.* . **82**, 13471352.

Hooft, E. E., Toomey, D. R. & Solomon, S. C., 2003, Anomalously thin transition zone beneath the Galápagos hotspot, *Earth Planet. Sci. Lett.*. **216**, 55-64.

Johnson, C. E. & Hadley, D. M., 1976, Tectonic implications of the Brawley earthquake swarm, Imperial Valley, California, January 1975, *Bull. Seism. Soc. Am.* **66**, 1133-1144.

Jordan, T. H., 1991, Far-field detection of slow precursors to fast seismic ruptures, *Geophys. Res. Lett.*. **18**, 2019-2022.

Kagan, Y. Y., and L. Knopoff, 1991, Stochastic synthesis of earthquake catalogs, *J. Geophys. Res.*. **86**, 2853 2862.

Kanamori, H., & Anderson, D. L., 1975, Theoretical basis of some empirical relations in seismology, *Bull. Seism. Soc. Am.* **65**, 1073-1095.

Kilgore, B. D., Blanpied, M. L. & Dieterich, J. H., 1993, Velocity dependent friction of granite over a wide range of conditions, *Geophys. Res. Lett.*. **274**, 355-360.

King, C. Y., Nason, R. D. & Tocher, D., 1973, Kinematics of Fault Creep, *Phil. Trans. Roy. Soe. London, Ser. A. 274*. **274**, 355-360.

Linde, A. T., Gladwin, M. T., Johnston, M. J. S., Gwyther, R. L. & Bilham, R. G., 1996, A slow earthquake sequence on the San Andreas fault, *Nature*. **383**, 65-68.

Llenos, A. L., & McGuire, J. J., 2008, Modeling Seismic Swarms Triggered by Aseismic Transients, *submitted to Earth Planet. Sci. Lett.*

Lohman, R. B. & McGuire, J. J., 2007, Earthquake swarms driven by aseismic creep in the Salton Trough, California, *J. Geophys. Res.*. **112**(B04405), doi: 10.1029/2006JB004596.

Lyons, S. & Sandwell, D., 2003, Fault creep along the southern San Andreas from interferometric synthetic aperture radar, permanent scatterers, and stacking, *J. Geophys. Res.*. **108**(B1), doi:10.1029/2002JB001831.

Lyons, S.N. Bock, Y. & Sandwell, D.T., 2002, Creep along the imperial fault, southern California, from GPS measurements, *J. Geophys. Res.*. **107**(B10), doi: 10.1029/2001JB000763.

Magistrale, H., Day, S., Clayton, R. W. & Graves, R., 2000, The SCEC southern California reference three-dimensional seismic velocity model Version 2, *Bull. Seism. Soc. Am.* **90**, S65-S76.

McGuire, J. J., 2008, Seismic cycles and earthquake predictability on east pacific rise transform faults , *Bull. Seism. Soc. Am.* **98**, 1067-1084.

McGuire, J. J., Boettcher, M. S. & Jordan, T. H., 2005, Foreshock sequences and short-term earthquake predictability on East Pacific Rise transform faults, *Nature*. **434**, 457-461.

Nishimura, C. E. & Forsyth, D. W., 1988, Rayleigh wave phase velocities in the Pacific with implications for azimuthal anisotropy and lateral heterogeneities, *Geophys. J.* **94**, 479-501.

Ogata, Y., 2005, Detection of anomalous seismicity as a stress change sensor, *J. Geophys. Res.*. **110**(B5), doi: 10.1029/2004JB003245.

Ogata, Y., 1988, Statistical models for earthquake occurrences and residual analysis for point processes, *J. Am. Stat. Assn.*. **83**, 9-27.

Omori, F., 1894, On the aftershocks of earthquakes, *J. Coll. Sci. Imp. Univ. Tokyo*. **7**, 111-200.

Richter, C. F., 1958. *Elementary Seismology*. W. H. Freeman, San Francisco, Ca.

Rubin, A. M. Ampuero, J., 2007. *Slow-Slip Propagation Speeds*. *AGU Fall Meeting Abstracts* B1.

Shapiro, S. A., Rentsch, S., & Rothert, E., 2005, Characterization of hydraulic properties of rocks using probability of fluid-induced microearthquakes, *Geophysics*. **70**, F27-F33.

Shearer, P. M., Hauksson, E. & Lin, G., 2005, Southern California Hypocenter Relocation with Waveform Cross-Correlation, Part 2: Results Using Source-Specific Station Terms and Cluster Analysis, *Bull. Seism. Soc. Am*. **95**, 904-915.

Shearer, P. M., 1997, Improving local earthquake locations using the L1 norm and waveform cross correlation: Application to the Whittier Narrows, California, aftershock sequence, *J. Geophys. Res*. **102**, 8269-8283.

Shibazaki, B. & Shimamoto, T., 2007, Modelling of short-interval silent slip events in deeper subduction interfaces considering the frictional properties at the unstablestable transition regime, *Geophys. J. Int.*. **171**, 191-205.

Smith, K. D., von Seggern, D., Blewitt, G., Preston, L., Anderson, J. G., Wernicke, B. P. & Davis, J. L., 2004, Evidence for deep magma injection beneath Lake Tahoe, Nevada-California, *Science*. **305**, 5688.

Stein, R. S., 1999, The role of stress transfer in earthquake occurrence, *Nature*. **402**,605-609.

Trèhu, A. M., & Solomon, S. C., 1983, Earthquakes in the Orozco transform zone; Seismicity, source mechanisms, and tectonics , *J. Geophys. Res*. **88**, 8203-8225.

Vidale J. E. & Shearer, P. M., 2006, A survey of 71 earthquake bursts across southern California: Exploring the role of pore fluid pressure fluctuations and aseismic slip as drivers, *J. Geophys. Res.*. **111**(B05312), doi:10.1029/2005JB004034.

Vidale J. E., Boyle, K. L. & Shearer, P. M., 2006, Crustal earthquake bursts in California and Japan: Their patterns and relation to volcanoes, *Geophys. Res. Lett*. **33**(L20313), doi:10.1029/2006GL027723.

Waldhauser, F. & Ellsworth, W. L., 2000, A Double-Difference Earthquake Location Algorithm: Method and Application to the Northern Hayward Fault, California , *Bull. Seism. Soc. Am*. **90**, 1353-1368.

Figure 1. Strike-slip focal mechanisms from Global Centroid Moment Tensor (CMT) solutions representative of the three oceanic transform fault earthquakes analyzed here: EPR sequences from the Siqueiros (SIQ-2001) and Gofar (GOF-2007) transform faults, as well as the Galapagos Ridge transform (GAL-2000). Inlay map displays Southern California seismicity, including focal mechanisms representative of four Salton Trough swarms: Obsidian Buttes, West Moreland, Imperial Fault and Brawley swarms (focal mechanisms clockwise from northeast). Dots show Southern California locations of seismic bursts identified by Vidale and Shearer (2006) as swarm-like (red dots) and those identified as aftershock sequences (black).

Figure 2. Earthquakes associated with swarms are displayed here in terms of their time and moment magnitude, with time in hours relative to the largest event. Similar triggering patterns are apparent. Several sequences display their largest events occurring several hours after the onset of increased seismicity. All seven sequences, including those that begin with their largest events, deviate from established earthquake triggering models.

Figure 3. 1981 West Moreland swarm. ***a.)*** Moment magnitude (M_w) versus time, in hours, from the onset of increased seismicity rate. ***b.)*** Event locations derived from *HypoDD* double-difference arrival time relocation algorithm (Lohman & McGuire 2007). Bilateral hypocentral migration can be observed, spreading outward along the fault during the period of highest seismicity rate, then moving northward late into the sequence. ***c.)*** Along fault migration rates are between 0.5 and 1.0 km/hr. In all plots, color indicates relative occurrence time of individual event in the sequence.

Figure 4. 2005 Obsidian Buttes swarm. ***a.)*** Earthquake moment magnitude versus time. ***b.)***Event locations derived from *HypoDD* double-difference arrival time relocation algorithm (Lohman & McGuire 2007). ***c.)*** During the swarm, hypocenters migrate bilaterally along the NE-trending fault at a rate between 0.1 and 0.5 km/hr. Color corresponds to relative time of event.

Figure 5. 2003 Imperial Fault Swarm. ***a.)*** Moment magnitude versus time displays a nearly symmetric temporal moment release pattern, with small magnitude seismicity ramping up to the largest event 10 hours into the sequence. ***b.)*** Event locations derived from *HypoDD* double-difference arrival time relocation algorithm using data from SCEC (California) and RESNOM (Mexico) seismic arrays. ***c.)*** Hypocenters migrate unilaterally along the NE-trending fault from the southwest to the northeast at rates between 0.1 and 0.5 km/hr. Color corresponds to time of event.

Figure 6. Locations of events associated with the 2000 Galapagos sequence derived from R1 surface-waves ***(a)***. Three example centroid location inversion figures are also shown here ***(b, c, d)***. The empirical Green's function cross-correlation technique used to identify arrivals with similar focal mechanisms in seismograms from GSN stations is illustrated in the upper panel of each location figure. Blue lines represent the bandpass-filtered EGF waveform at each station, red lines represent waveforms of the event being located. Locations are derived by fitting a cosine function to relative arrival time delays from a set of azimuthally distributed stations (shown in lower panels). Azimuth and distance relative location information derived from the cosine fit is illustrated by comparing the cosine phase and amplitude of events located north ***(b, c)*** of the Greens function event, shown as the black star, to those located to the south ***(d)***.

Figure 7. 2000 Galapagos Swarm ***a.)*** Black symbols correspond to times and magnitudes derived from Love-wave cross-correlation using data from the seismometer array on the Galapagos Islands. Colored symbols correspond to events relocated using teleseismic R1 surface-wave data. ***b.)*** Derived centroid locations for events along the transform fault demonstrate migration from south to north during the swarm at rates ***(c)*** of approximately 1.0 km/hr. Color in all plots indicates time of event.

Figure 8. 2001 Siqueiros transform sequence. ***a.)*** Time and magnitudes and ***b.)*** locations derived from surface-wave relocation technique, displayed here as colored symbols. Black dots represent t-phase data from the NOAA hydroacoustic catalog. Earthquakes occurred on two fault segments with a complicated temporal-spatial evolution. ***c.)*** During this sequence, seismicity migrated from west to east along both segments at variable rates, moving from the eastern segment to the western segment during the late stages of the sequence. Color corresponds to time of event.

Figure 9. 2007 Gofar Swarm ***a.)*** Time-magnitude of 13 large events and ***b.)*** locations are derived using R1 surface-wave location technique. ***c.)*** Event centroid locations appear to migrate along the eastern segment of the Gofar transform from west to east at a rate on the order of 1 km/hr. Color corresponds to time of event.

Figure 10. Comparison of calculated values of the skew of seismic moment release history and effective seismic stress drop for each of the 7 sequences presented here along with those from the Vidale and Shearer (2006) analysis of seismic bursts in Southern California. Oceanic transform events (blue stars) as well as continental transform events from the Salton Trough (brown stars) trend toward the low skew-low stress drop quadrant of the parameter space, especially compared to values associated with aftershock sequences (stress drop $\sim$10 MPa, positive skew). Circles are from the Vidale and Shearer study, and are also consistent with this trend; grey circles represent aftershock sequences and red circles represent sequences determined to be swarm-like.

Figure 11. ETAS-transformed time versus cumulative number of events that occurred on the Galapagos Ridge transform fault from May 1999 to September 2002. The seismicity rate predicted by the ETAS model is dependent on the time elapsed since the last event as well as the occurrence times and magnitudes of other previous events and the background seismicity rate (Ogata 1988). Maximum likelihood estimates of ETAS parameters derived here ($\mu = 0.03$, $c = 0.01$ and $k = 0.3$) are optimized for the first 26 month time period with p and α constrained to 1.0 and 0.8 respectively. We assume a lower magnitude threshold of M_w3.6. The best fit ETAS parameters are used to extrapolate the predicted cumulative number of events for the entire data set (red line). Blue line represents actual data. A significant deviation from the ETAS prediction is associated with the two-day earthquake swarm in October of 2000 (shaded region). The occurrence of largest event of that sequence, a M_w5.9 at 15:53 on October 21st, is indicated with dotted line. Grey lines represent the 2σ confidence interval for the extrapolation of the ETAS prediction beyond the optimization time period, assuming a standard Brownian process with a linear trend slope of 1 (Ogata 2005).

Table 1. Southern California and RTF Swarm Seismicity Parameters

SEQUENCE	SKEW	TOTAL M_w	BURST RADIUS	STRESS DROP	APPROX. MIGRATION RATE	
BRAWLEY1975	+20	5.04	4.5 km	0.2 MPa	∼0.5 km/hr	(Johnson & Hadley 1976)
WEST MORELAND1981	-17	5.80	6.03 km	1.28 MPa	∼1.0 km/hr	(Lohman & McGuire 2007)
OBSIDIAN BUTTES 2005	-8	5.27	2.28 km	3.75 MPa	∼0.5 km/hr	(Lohman & McGuire 2007)
IMPERIAL 2003	-2	3.84	1.2 km	0.18 MPa	∼0.5 km/hr	*(this study)*
GALAPAGOS 2000	-4	5.89	11.5 km	1.0 MPa	∼1 km/hr	*(this study)*
SIQUEIROS 2001	+5	5.85	12.2 km	1.5 MPa	UNCERTAIN	
GOFAR 2007	+4	5.05	5.2 km	0.2 MPa	∼1 km/hr	*(this study)*

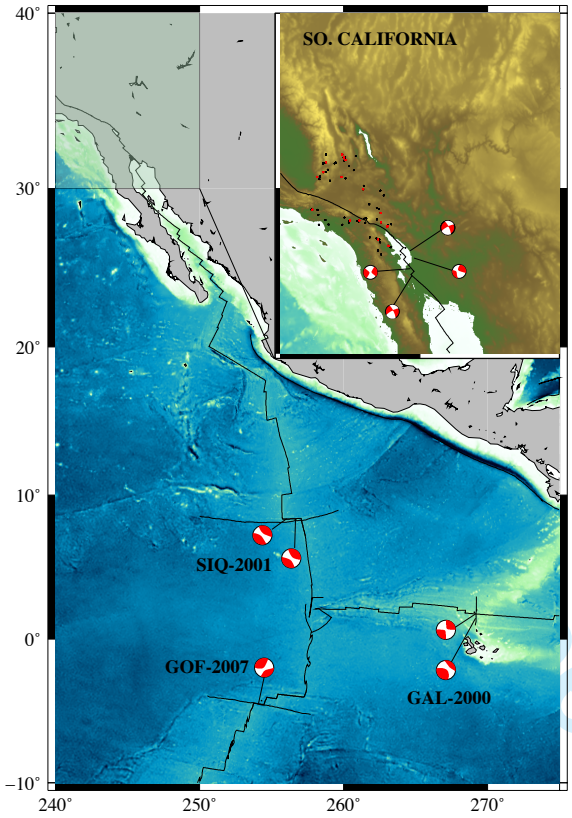

Figure 1.

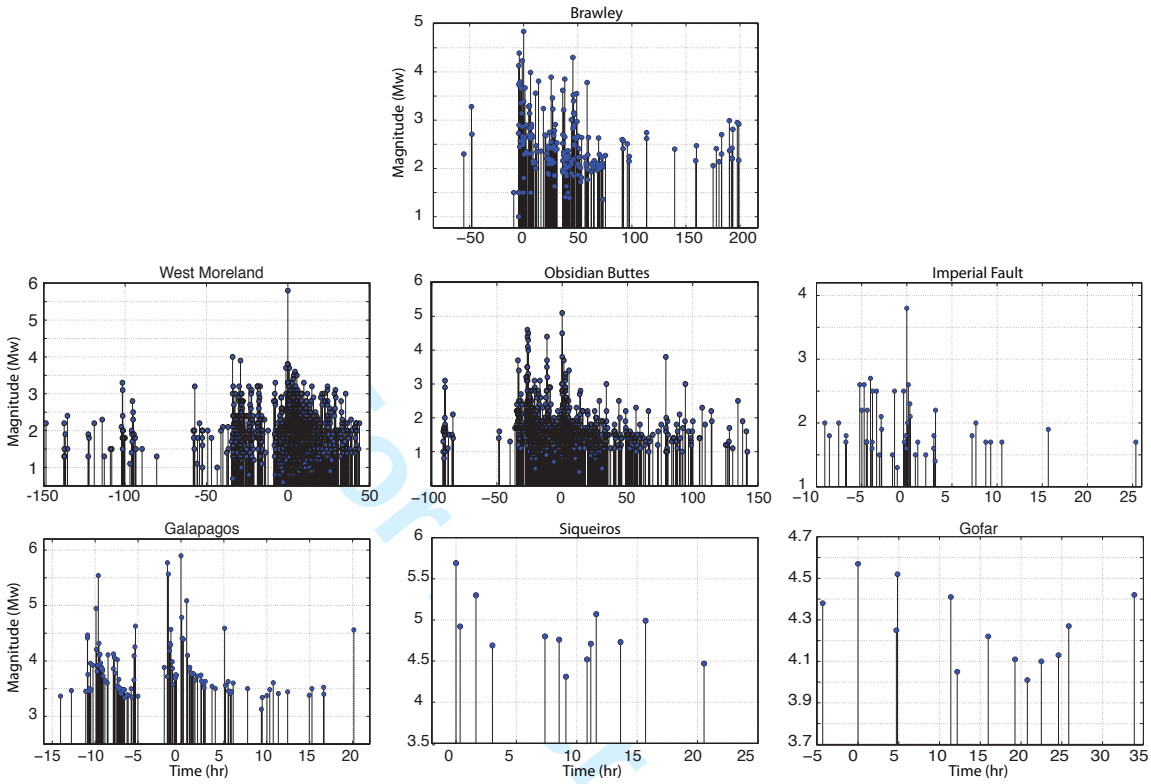

Figure 2.

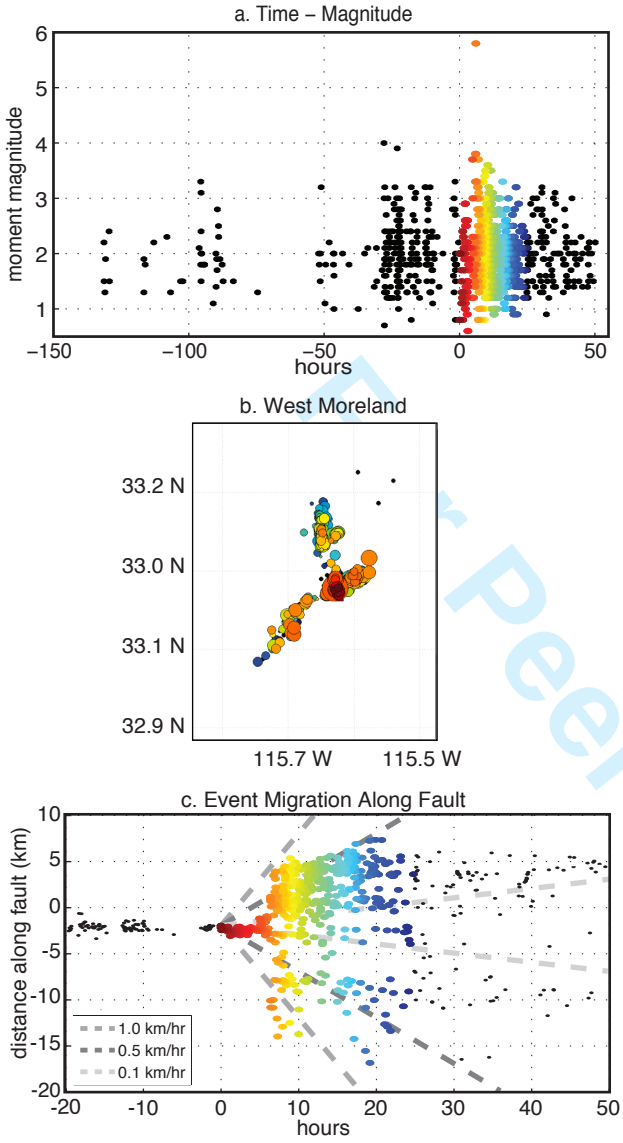

Figure 3.

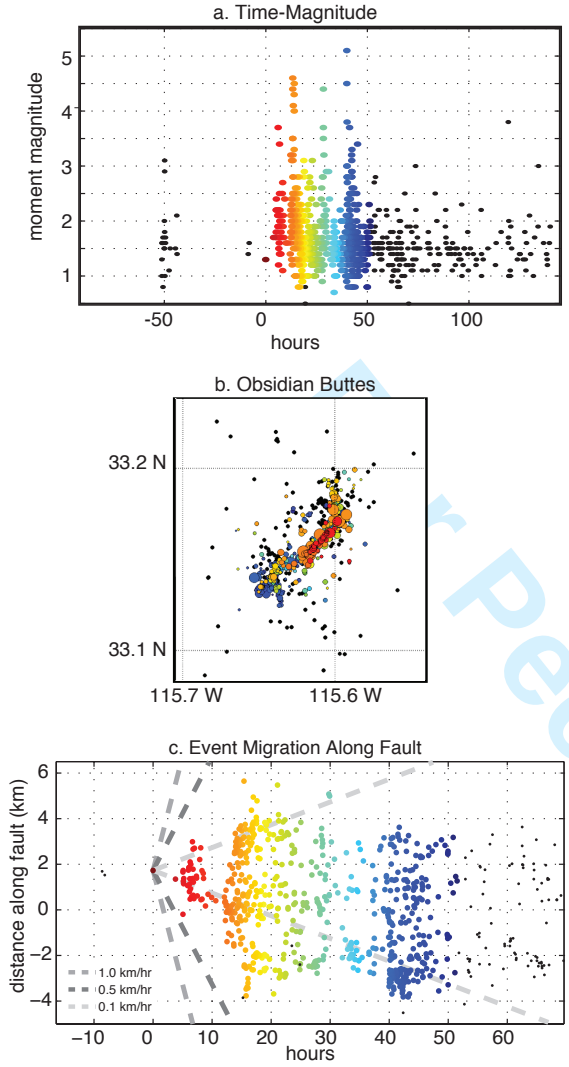

Figure 4.

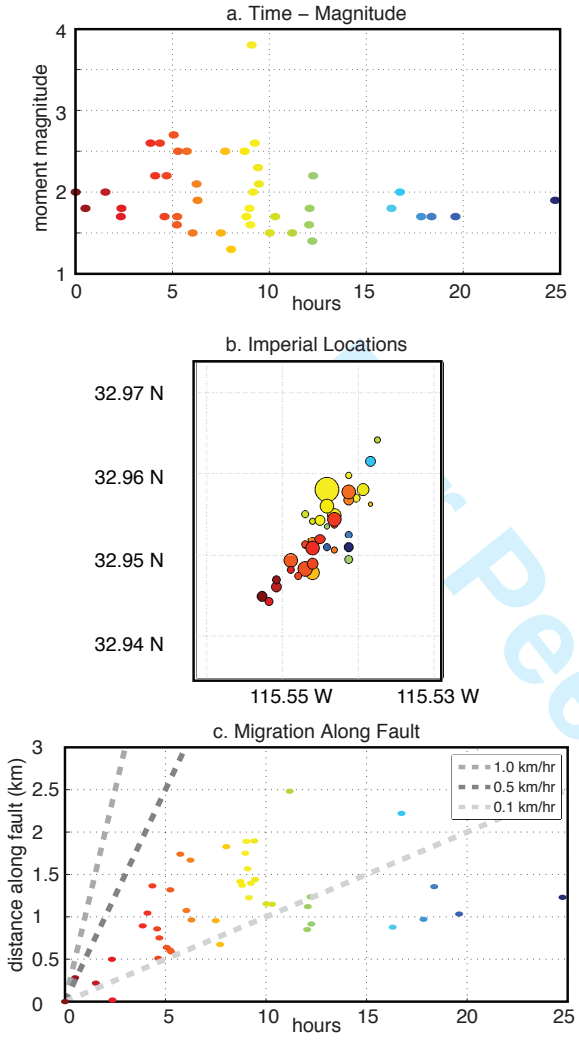

Figure 5.

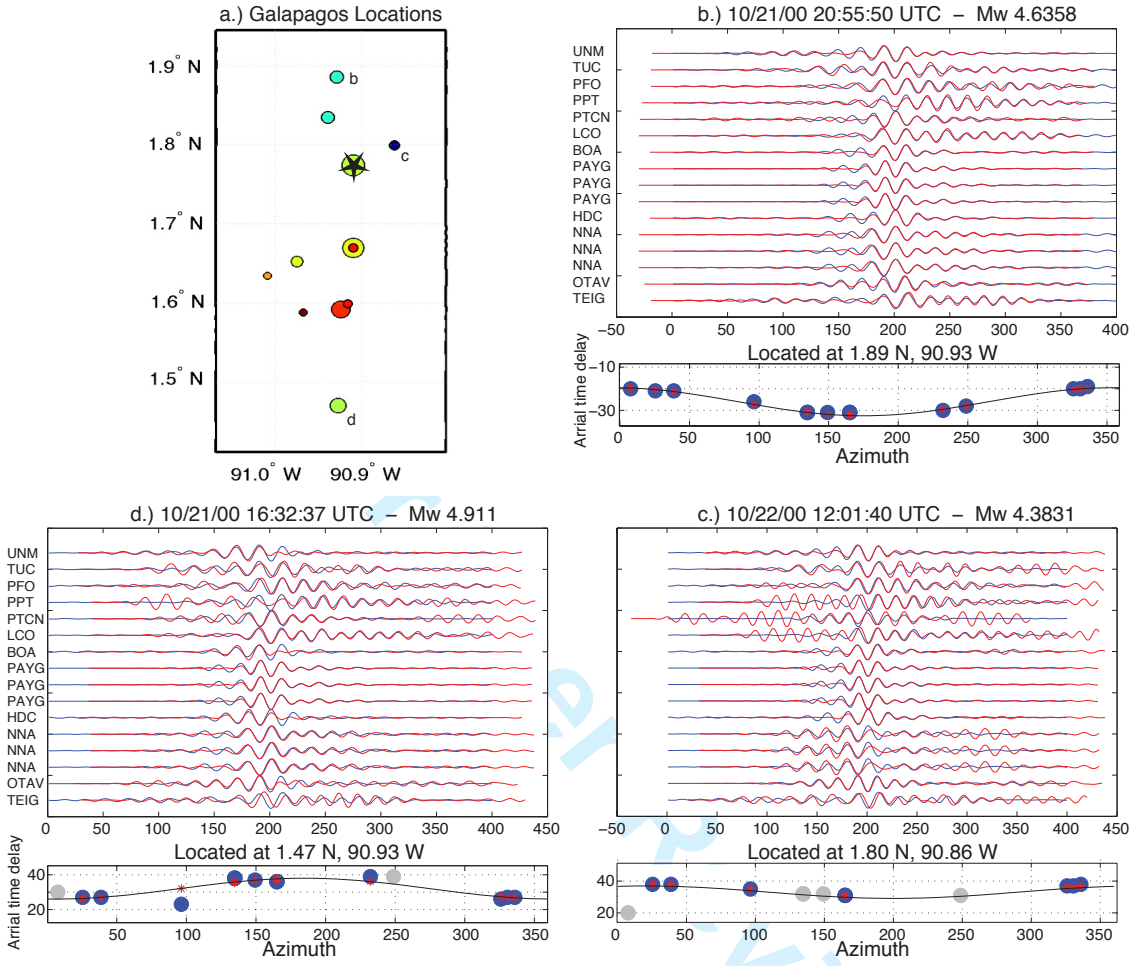

Figure 6.

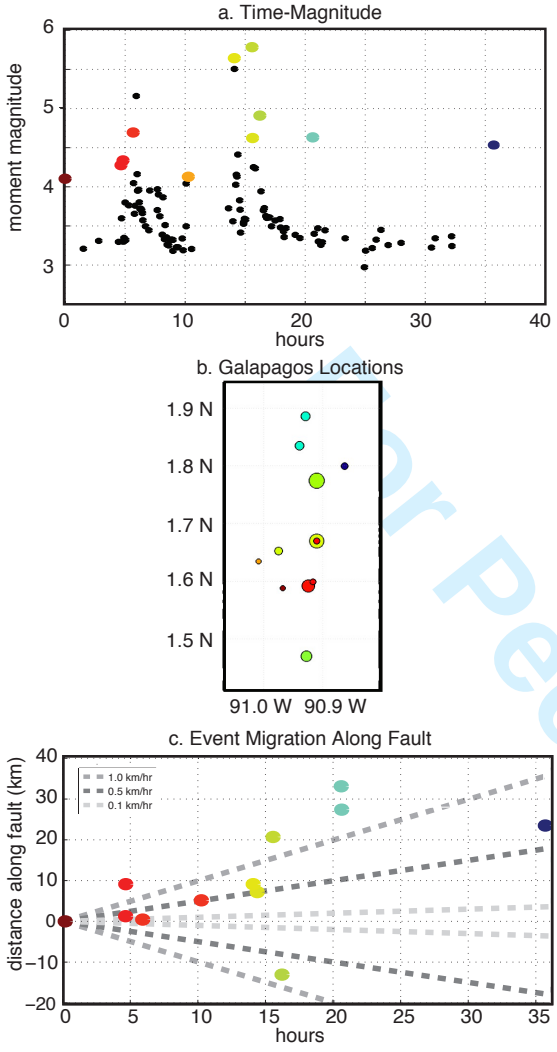

Figure 7.

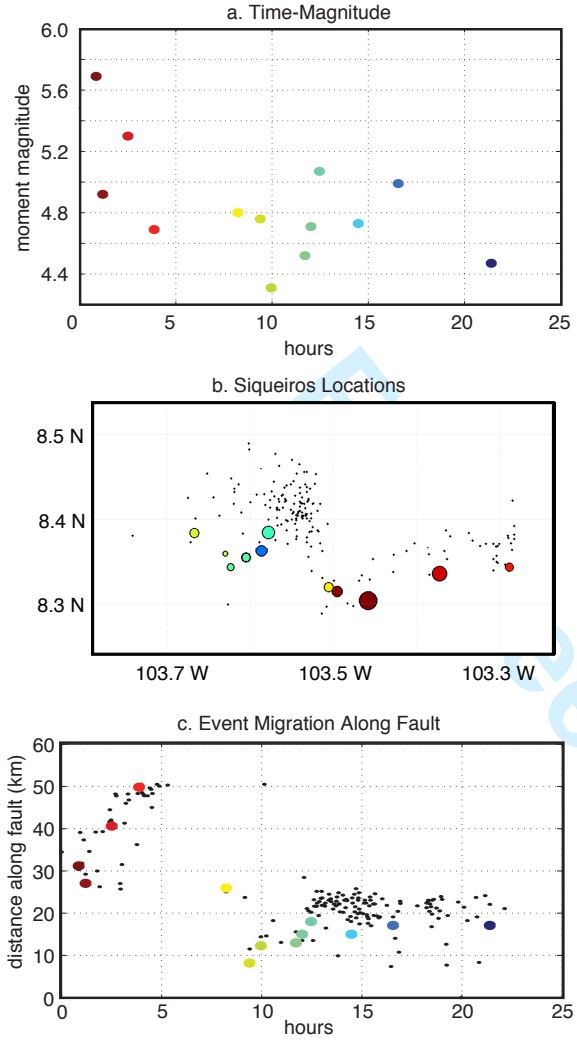

Figure 8.

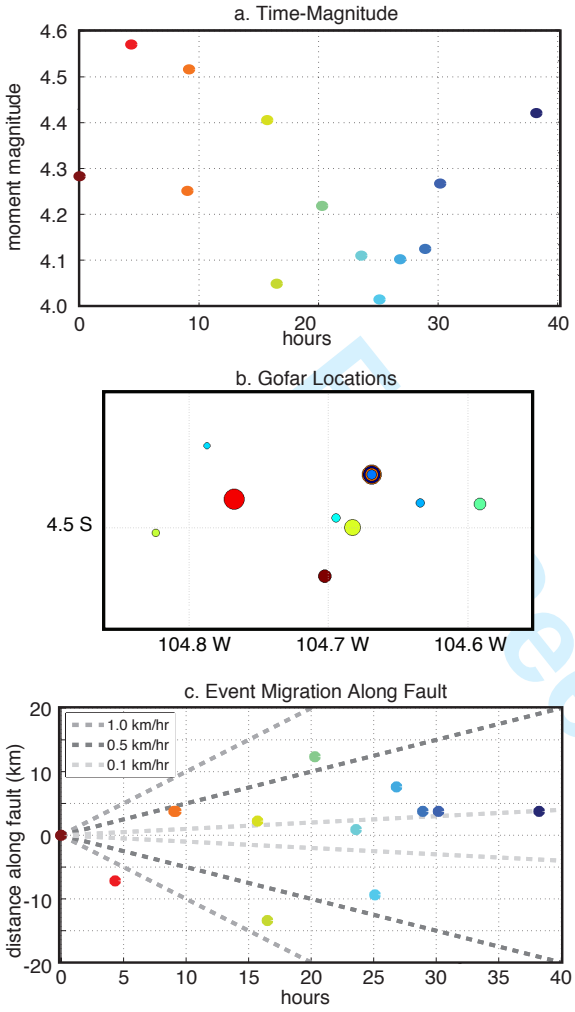

Figure 9.

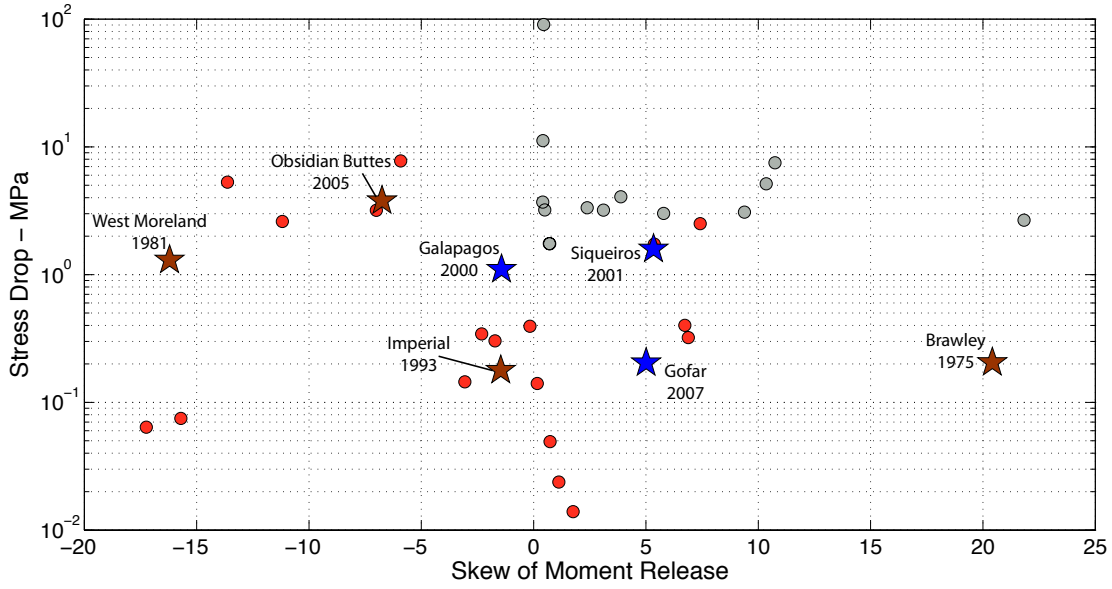

Figure 10.

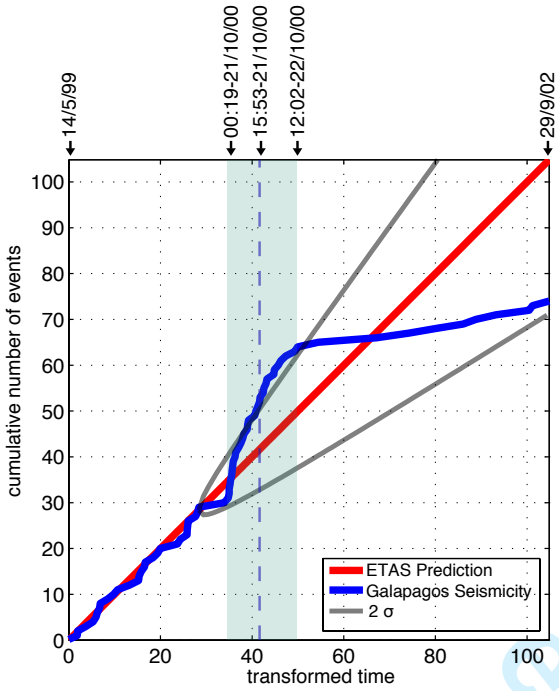

Figure 11.